



# Evaluation of the influence of ultrasonic vibration on physical, tensile, and morphological properties of fused deposition modeled specimens

Raihan Quader<sup>1</sup> · Leo Klinstein<sup>2</sup> · David Grewell<sup>3</sup> · Lokesh Karthik Narayanan<sup>1</sup>

Received: 6 December 2023 / Accepted: 8 March 2024 / Published online: 19 March 2024  
© The Author(s) 2024

## Abstract

The use of fused deposition modeling (FDM) in printing polymers for various applications has been ever increasing. However, its utilization in printing polymers for high-strength and superior surface finish applications is still a challenge, primarily due to process intrinsic defects, i.e., voids between the layers and the rough exterior arising from unrestrained deposition of molten polymer. This research hypothesizes that application of ultrasonic vibration (USV) post-fabrication could minimize these shortcomings. For this investigation, ASTM D638 Type IV samples were FDM-printed using poly(lactic) acid (PLA). Through screening experiments, an optimized set of ultrasonic parameters was determined. Then, the effect of both-sided ultrasonic application was characterized. Subsequently, the impact of USV on the samples' physical, tensile, and morphological properties was examined by varying the layer height, infill patterns, and % infill density. Up to 70% roughness reduction was observed as a result of post-FDM ultrasonic application. Additionally, the tensile strength of the samples increased by up to 15.31%. Moreover, for some lower % infill samples, post-ultrasonic tensile strengths were higher than 100% infill control samples. Analysis of scanning electron microscopy (SEM) and X-ray computed tomography (CT) imagery indicated enhanced layer consolidation and reduced void presence in samples treated with ultrasonic. The combination of ultrasonic-generated heat and downward pressure promoted a synergistic squeeze flow and intermolecular diffusion across consecutive layers of polymers. As a result, increased tensile strength and surface finish were achieved while dimensional change was marginal.

**Keywords** Ultrasonic vibration · Fused deposition modeling · Tensile properties · Interlayer adhesion

## 1 Introduction

Fused deposition modeling (FDM) is the most widely used additive manufacturing (AM) method owing to its simple operation, cost-effective equipment, affordable materials,

and minimal need for process monitoring. Through FDM, parts with intricate shapes can be produced with high precision with less weight than other net-shaping processes. FDM is also an efficient process in terms of cost and time as it generates low waste and does not involve complex process planning [1, 2]. However, FDM has limitations that prevent its use in high-volume and high-strength applications. Major limitations include anisotropy in the Z-direction, interlayer voids, weak interlayer adhesion due to insufficient polymer chain entanglement, and a stepped surface finish inherent to the process [3–5]. To overcome these challenges, there have been various strategies that have been proposed and evaluated [6].

In FDM, polymer filament is fed into a heated extruder that melts and extrudes the polymer, which is then deposited layer by layer along a predetermined path to build the designed 3D geometry [7]. However, this free-flowing deposition leads to the creation of voids between the layers as the material is deposited in an elliptical shape without any external force [8]. Moreover, during the deposition of a new

✉ Lokesh Karthik Narayanan  
lokesh.narayanan@ndsu.edu

Raihan Quader  
raihan.quader@ndsu.edu

Leo Klinstein  
lklinstein@dukane.com

David Grewell  
dgrewell@niu.edu

<sup>1</sup> Department of Industrial and Manufacturing Engineering,  
North Dakota State University, Fargo, ND 58102, USA

<sup>2</sup> Dukane Corporation, St. Charles, IL 60174, USA

<sup>3</sup> College of Engineering and Engineering Technology,  
Engineering Building, DeKalb, IL 60115, USA

layer, the temperature of the previous layer is often near or below the glass transition temperature, resulting in weak polymer chain entanglement between the layers [9]. The combination of these voids and weak interlayer adhesion negatively impacts the mechanical properties of the finished parts. In addition, the elliptical deposition of molten polymer layer after layer creates a wavelike undulating surface finish on external sides which limits the usage of FDM-generated parts in applications that require smooth surface finish. Researchers have attempted different pre-, in situ, and post-processing techniques to reduce voids and enhance interlayer adhesion as well as surface finish [5].

Khurana et al. employed finite element analysis (FEA) to determine layer paths and shapes based on principal stress trajectories as a pre-processing step. The FEA stress data were integrated into a slicer software to generate 3D layers. The samples printed using this method exhibited improved results in the 3-point bend test [10]. Narahara et al. investigated the use of atmospheric pressure plasma during printing to enhance the bond strength between the layers. The application of plasma radiation aided in increasing the rupture stress of the printed samples [11]. Kishore et al. used infrared preheating in big-area additive manufacturing (BAAM) to improve interlayer adhesion. By heating the previously printed layer with infrared just before depositing the new layer, they achieved better fracture energy [12]. Ravi et al. replaced infrared heating with laser heating before printing each layer which resulted in a 50% increase in interlayer bond strength [13]. Another method that has been explored in recent years to increase the strength of FDM parts is ultrasonic welding.

Ultrasonic welding is a widely used fast-joining technique for plastic parts of different designs made from various thermoplastics. Even polymer composites and dissimilar polymers can be welded together using ultrasonic vibration. In this technique, ultrasonic vibration (USV) is applied to join two different parts at their interfaces. Energy directors or surface asperities can be utilized to concentrate the ultrasonic energy at the mating surface and facilitate melting for joining purposes [14]. A typical ultrasonic stack assembly consists of a transducer, booster, and horn. By varying the booster type and horn geometry, different end amplitudes can be produced depending on the requirement of specific materials and joint types [15]. Therefore, USV can be a suitable post-processing technique for FDM parts.

Since FDM builds parts layer by layer, each layer can be perceived as an individual entity. In FDM, at the interfaces of two layers, the intermolecular chain entanglement is significantly lower than any other net-shaping processes (i.e., injection molding, compression molding) [16]. It is hypothesized that applying a combination of USV and downward force can soften the polymer at the interface between these layers. The softened polymer could flow into the voids and enhance

intermolecular chain entanglement. This flow under USV and downward force is called squeeze flow. On removal of this USV, the polymer rasters can solidify into a denser structure through an increased interfacial healing phenomenon. This process could improve the mechanical strength of the parts and result in a smoother surface.

Li et al. employed USV as a post-processing technique to enhance the mechanical, thermal, and physical properties of FDM parts [17]. They used a controlled variate method to study the effect of main ultrasonic parameters while keeping power and frequency constant. They found that strengthening pressure and weld time had a significant impact on the properties of FDM samples. However, they did not consider different booster types, applying USV on both sides, the relationship between USV and different layer heights, infill patterns, and the density of FDM samples. Additionally, depending on the manufacturer of ultrasonic welding equipment, the welding parameters and methods can vary. In our previous study, USV was applied on both sides of the completed FDM prints using “energy” and “peak power” modes in a Dukane system where the FDM parameters were kept constant [18]. We observed a maximum 12% increase in tensile strength while the surface roughness was significantly decreased.

In this study, we have used the “distance” mode of ultrasonic application for all experiments to evaluate its effect compared to the other modes studied previously [18]. At first, we performed a parameter screening for ultrasonic-booster type, collapse distance, and velocity of the ultrasonic stack to observe corresponding effects on tensile strength. Next, a similar screening was performed for trigger force (TF). Following the identification of the optimum parameters, the impact of USV on one side and both sides of FDM parts was characterized using X-ray computed tomography (X-ray CT). The X-ray CT images proved that applying ultrasonic on both sides was beneficial in reducing the voids more. After that, the ultrasonic parameters were kept constant and FDM parameters (layers height, infill pattern, and infill density) were changed multiple times to characterize the combined effect of USV and FDM parameters on the tensile strength, average surface roughness, and thickness of the tested specimens. Scanning electron microscopy (SEM) and X-ray CT were utilized to examine the impact of USV on interlayer adhesion and voids inside the samples. The next section will explain the squeeze flow and increased interfacial healing through a physics-based model following established process models found in the literature.

## 2 Ultrasonic-induced integrated squeeze flow and intermolecular diffusion model

Different thermoplastics and their composites can be bonded through ultrasonic welding which is generally the application of high-frequency and low-amplitude

mechanical vibrations on the parts to be joined. Heat is generated at the mating surface because of the intermolecular friction caused by the vibration [19]. Thermoplastics are classified as viscoelastic substances, which means that when exposed to USV, a portion of the energy is converted into heat due to friction between the molecules. Studies have demonstrated that only the energy of the loss modulus is dissipated, while the storage modulus remains unaffected throughout this process. To determine the required ultrasonic energy for successfully melting the material, the yield strain of the material also needs to be considered. Equation (1) can be used to calculate the average amount of ultrasonic energy dissipated per unit of time in a certain material [19, 20].

$$Q_{avg} = \frac{\omega \epsilon_o E \epsilon}{2} \tag{1}$$

Here,  $\epsilon_o$  (yield strain) and  $E \epsilon$  (loss modulus) are constant values for a particular material but ultrasonic frequency  $\omega$  can be varied to obtain the  $Q_{avg}$  (required ultrasonic energy dissipated per unit of time) for ensuring adequate melting at the parts' mating surface.

It was previously mentioned that the welding can happen either by surface asperities or built-in energy directors. The dissipated energy softens these enough so that flow of material is possible and when combined with the applied downward vertical force by ultrasonic stack, the actual flow occurs followed by the formation of weld area upon removal of USV. This phenomenon is termed “squeeze flow” [21]. In the current study, test specimens are printed using FDM and the schematic cross-section of the two consecutive layers can be expressed by Fig. 1(a). Half of the areas from such adjacent layers can be considered a collection of surface asperities. We hypothesize that when USV is applied, these asperities soften and lead to the occurrence of squeeze flow. Grewell et al. put forth a model that conceptualized the idealized squeeze flow, where the surface asperities were represented as small

cylindrical shapes of molten polymer situated between two rigid plates, with a distance of  $2h$  separating them (as illustrated in Fig. 1(d)). To simplify the model, only one surface asperity was considered in the mathematical model [21]. Bird et al. proposed a similar model and provided Eq. (2) with which the pressure ( $p$ ) can be expressed as a function of time ( $t$ ) [22].

$$p = \frac{3\mu}{4h^3} \frac{\partial h}{\partial t} (r^2 - r_{od}^2) \tag{2}$$

Here,  $\mu$  is Newtonian fluid viscosity,  $h$  is the height of one molten asperity peak,  $r$  is the radius of molten asperity peak at time  $t$ , and  $r_{od}$  is the final radius. To find the required force ( $F$ ) to close the gap  $h$ , Grewell et al. performed further investigation and presented Eq. (3) [21].

$$\frac{h_o}{h(t)} = \left( \frac{16\pi F h_o^2}{3\mu r_o^4} t + 1 \right)^{1/4} \tag{3}$$

Here,  $h_o$  is the original height of asperity peak and  $r_o$  is the original radius. Using this equation, the gap height or the closing of the two mating surfaces can be predicted as a function of time. It should be noted that the gap is proportional to time raised to the power of 1/4th.

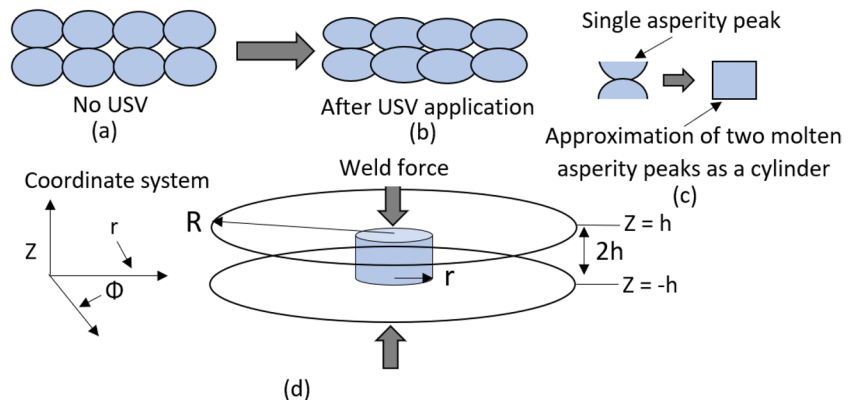
The interfacial healing of polymer chains starts immediately after squeeze flow occurs. At the weld area, the intermolecular chain entanglement increases through polymer chain diffusion. Figure 2 illustrates the interfacial healing process at various time durations.

DeGennes used the reptation theory to model the diffusion of polymer chains where he visualized a polymer chain inside an imaginary tube [23, 24]. Diffusion distance was defined as the distance a chain travels along the tube. He related the square of diffusion distance  $\langle l \rangle^2$  to time  $t$  with the following equation

$$\langle l \rangle^2 = 2D_c t \tag{4}$$

Equation (4) shows that the square of the distance a polymer chain travels due to diffusion is proportional to time

**Fig. 1** Cross-section visualization of FDM layers; (a) no USV, (b) after USV application, (c) conceptual asperity peak, and (d) idealized squeeze flow model (reproduced with permission from Grewell et al. [21])



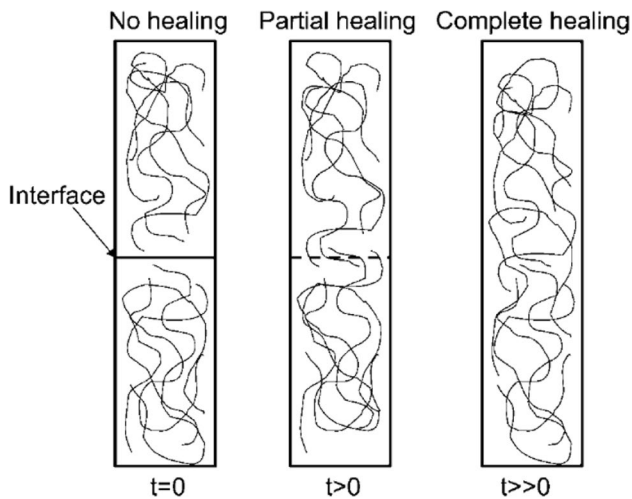


**Fig. 2** Relationship of polymer chain diffusion and interfacial healing with time [21]

where  $D_c$  is the diffusion constant. He also showed that the end-segment motion of a chain outside the tube is easier than the internal segments because the internal segments' movements were restricted by the constraints of surrounding chains. Equation 5 was proposed to relate the two different distances  $\langle l \rangle$  and  $X$  where  $X$  is the distance a chain advances across the interface for healing.

$$X = \sqrt{\langle l \rangle} \quad (5)$$

Through further simplification of Eqs. 4 and 5, the following equations were obtained

$$X = 2D_c t^{1/4} \quad (6)$$

$$X \sim t^{1/4} \quad (7)$$

Equation (7) shows how healing can be related to time. If intermolecular diffusion and healing are assumed to be proportional to each other, then it can be derived that healing is proportional to time to the power of 1/4th.

According to Jud et al., the diffusion coefficient ( $D$ ) can be expressed as an Arrhenius function of temperature  $T$  as shown in Eq. (8) [25].

$$D(T) = D_c e^{\left[-\frac{E_a}{kT}\right]} \quad (8)$$

$E_a$  is activation energy and  $k$  is Boltzmann constant. From Eqs. 3 and 7, it can be noticed that both the squeeze flow and interfacial healing are related to time at the same degree. Because these two processes occur simultaneously and would be impossible to distinguish them separately, hence, Grewell et al. proposed combining these two phenomena into a single expression. He considered the effective activation energy to be temperature-dependent. As a result,

the accuracy of their proposed model increased. Because of temperature-induced material deformation in welding, the assumption of effective activation energy being temperature-dependent is justifiable [26, 27]. This relation can be expressed in an Arrhenius form by Eq. (9).

$$E_a(T) = A_0 e^{-k_a T} \quad (9)$$

Here,  $A_0$  is material constant and  $k_a$  is temperature parameter. Following the approach of Bastien et al., the degree of welding ( $DoW$ ) for isothermal conditions can be expressed by Eq. (10) [28].

$$DoW(t) = DoW_0 + \Gamma e^{\left[-\frac{E_a}{kT}\right]} * t^{1/4} \quad (10)$$

Here,  $DoW_0$  is the initial degree of welding and  $\Gamma$  is the combined coefficient for squeeze flow and interfacial healing. As welding happens for a certain duration at different temperature levels, the healing increases over the time duration at a fixed temperature until full healing is completed over the whole duration of welding. Thus, a particular temperature profile could be divided into time intervals ( $\Delta t$ ). If we assume no healing before welding, and the welding duration ranges from 0 to  $t'$ , the welding degree ( $WD$ ) for combined squeeze flow and interfacial healing can be expressed by the relationship shown in Eq. (11) [21].  $A_0$ ,  $\Gamma$ , and  $k_a$  can be experimentally calculated.

$$WD(T, t)_h = \sum_{t=0}^{t'} \Gamma * e^{-A_0 e^{-k_a T} / kT} * \Delta t^{1/4} \quad (11)$$

Equation (11) represents the combination of interfacial healing and squeeze flow in ultrasonic welding. The consideration of temperature dependency for activation energy in this proposed model was assumed to be the result of melt viscosity being dependent on the temperature of the material.

## 3 Experimental methods

### 3.1 Polylactic acid

Standard PLA-Natural 1.75 mm filament spools—NatureWorks Ingeo™ 4043D PLA (3D fuel, USA) were used in all the studies in this paper.

### 3.2 Fused deposition modeling

ASTM D638 Type IV specimens were printed in the XYZ orientation. For the ultrasonic parameter screening experiments, MakerBot Replicator Z18 desktop 3D printer (MakerBot, NY, USA) and MakerBot Print slicer were used to print the samples. 0.40-mm diameter nozzle was used and the printing temperature was set to 215 °C. For the screening

experiments, the FDM samples were printed on rafts with 0.20 mm layer height, 100% infill density, and a “diamond” infill pattern. For all the other experiments, LulzBot Taz Pro S desktop 3D printer (Fargo Additive Manufacturing Equipment 3D, ND, USA) and Cura LulzBot slicer were used. The nozzle diameter was 0.50 mm, the printing temperature was set to 215 °C, and the platform temperature was set to 60 °C. Samples were printed with rafts using different infill patterns, densities, and layer heights as shown in Table 1.

### 3.3 Ultrasonic vibration treatment



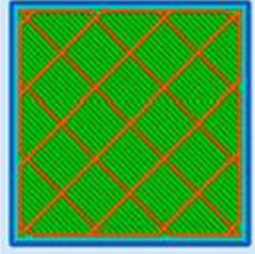
Ultrasonic vibration was applied on the FDM samples using a 20 kHz servo ultrasonic welding system (Dukane Corporation, St. Charles, IL). A custom fixture plate with a cavity matching the dimension of the ASTM D638 Type IV standard was machined to place the samples inside (Fig. 3(a)). An ultrasonic horn was machined with the bottom shape exacting the shape of the ASTM Type IV geometry (Fig. 3(b)). USV parameters were set up using the Dukane iQ Explorer II software. “Distance” mode of welding was used in all the experiments which was selected in the iQ Explorer II software. In this mode, after

the horn contacts the part, it goes down a user-specified “distance” generally known as the “collapse distance.” This ensures melting and welding of the same amount of material every time. This mode differs from the “energy” and “peak power” modes, where the USV application is controlled by the user-specified energy and peak power values generated by the system respectively.

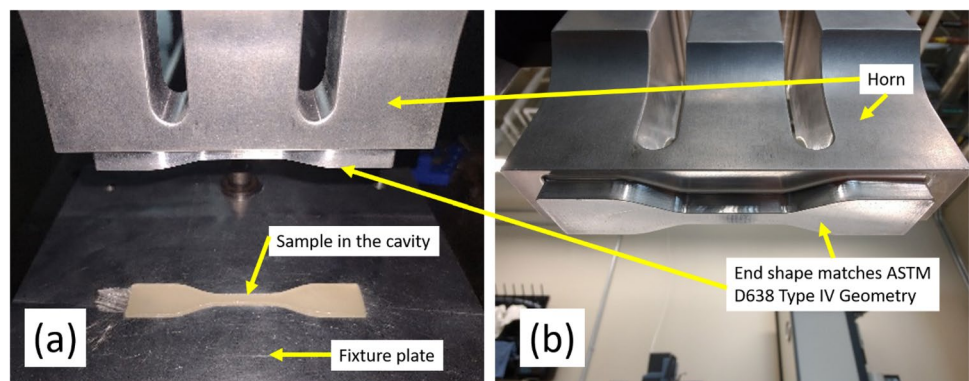
### 3.4 Surface roughness and thickness measurement

Surfcom surface texture measuring device was utilized to assess the average roughness of the top and bottom (raft side) surfaces of the ASTM samples before and after ultrasonic treatment. The measurements were recorded in microns (µm), while the vertical magnification and cutoff were set at ×2 K and 0.80 mm, respectively. To compare the thicknesses before and after ultrasonic application, the thicknesses of the samples were measured using a vernier caliper. In both measurement approaches, the gauge area of the samples was the area of interest. A sample size of  $n = 3$  was used.

**Table 1** FDM parameters for samples printed in LulzBot printer

Patterns			
	Lines	Zig-zag	Grid
	Infill density	80, 90, & 100%	
Layer height	0.20, 0.30, 0.40, 0.50 mm		

**Fig. 3** (a) Customized fixture plate with a cavity for placing sample; (b) customized horn with end shape exacting ASTM D638 Type IV geometry



### 3.5 X-ray CT

GE vltomelx s microCT system (GE, MA), which operates at 240 kV, was utilized to scan the ASTM samples before and after USV was applied. This non-invasive method of examining internal structures was employed to examine the impact of ultrasonic treatment on the deposited layers. To access and analyze the output files, myVGL viewer application was used.

### 3.6 Tensile test

Tensile property testing was carried out using an Instron 5567 mechanical testing machine (Instron, MA) with a 30 KN load frame. The “Extension” option was used as the test control and the crosshead speed was set to 5 mm/min. To measure the strain deformation, an MTS Model 632.11B-20 extensometer (MTS Systems Corp, MN) was utilized. A sample size of  $n = 3$  was used.

### 3.7 SEM imaging

Fracture surface morphology of the samples after the tensile test was observed using a JSM-6490LV scanning electron microscope (JEOL USA, MA). Small sections from the fracture area were cut and the fracture surface was sputter-coated with carbon before placing inside the SEM chamber. 15 kV of acceleration voltage and several magnifications were used to capture the fracture surface images.

### 3.8 Statistical analyses

Two-way analysis of variance (ANOVA) was performed considering the factors and their levels as illustrated in Table 2 for each of the response variables using JMP Pro 17 software ( $\alpha = 0.05$ , two-sided). The effect of the factor levels and their

interactions on the response variables were analyzed using the Tukey post hoc analysis ( $\alpha = 0.05$ , two-sided).

## 4 Results and discussion

### 4.1 Screening experiment of booster and ultrasonic parameters

Initially, a screening experiment was performed to characterize the effect of horn down speed, collapse distance, and different boosters on the tensile property of ASTM samples. A full factorial design of experiment was developed considering 4 down speeds, 3 collapse distances, and 2 booster types as shown in Table 3. In total, 72 samples were printed (36 for each booster type,  $n = 3$ ) and ultrasonic was applied only on one side of the samples using the defined set of parameters. A constant TF of 200 N was used for these runs.

Some of the parameter combinations created excessive flashes and deformed areas on the sample surfaces as presented in Fig. 4(a). In accordance to Eq. 11, the total degree of welding depends on the duration of welding and the temperatures at specific time intervals over the duration. If the time for traveling a specific collapse distance or the collapse distance itself was too high for the material being welded, over-welding could happen and could lead to deformed shapes and flashes. We believe that for some of the parameter combinations, over-welding occurred and the mentioned defects were observed. Those sets of samples were not tested for tensile properties. For 1:1 ratio booster, the tested sets of samples produced lesser tensile strengths than the control sample for all parameter combinations, but for 1:0.60 ratio booster, the tensile strengths were slightly higher than the control sample. This observation is aligned with a similar result shown in the work of Wen et al. where the effect of USV on plastic deformation

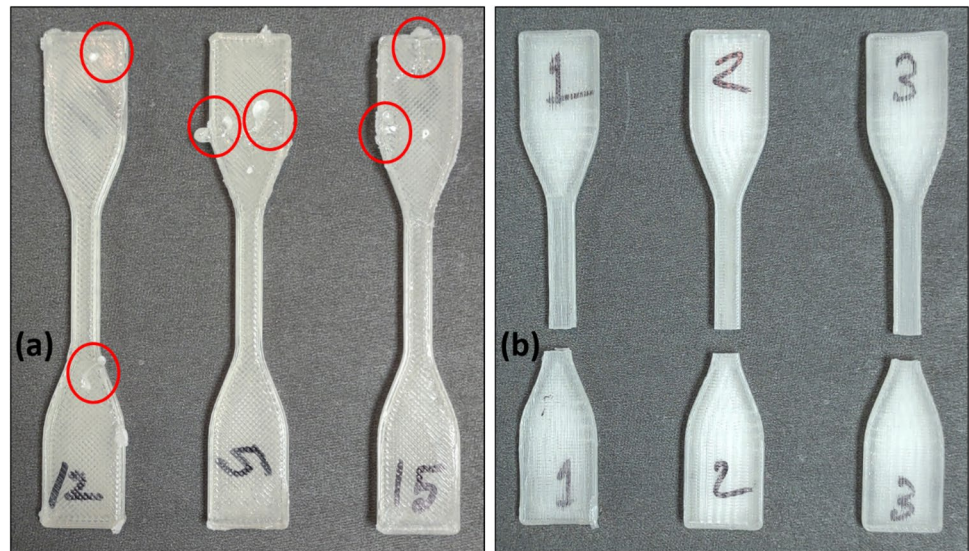
**Table 2** Factors, their levels, and the response variables for two-way ANOVA and the Tukey post hoc analysis

Response variables	Factor 1 (levels)	Factor 2 (levels)	Factor 3 (levels)	Factor 4 (levels)
Surface roughness	Infill pattern (lines, zig-zag, grid)	Infill density (80%, 90%, 100%)	Both-side USV application (no, yes)	Side of sample (top, bottom)
Thickness	Infill pattern (lines, zig-zag, grid)	Infill density (80%, 90%, 100%)	Both-side USV application (no, yes)	
Maximum tensile strength	Infill pattern (lines, zig-zag, grid)	Infill density (80%, 90%, 100%)	Both-side USV application (no, yes)	

**Table 3** Screening experiment parameters considering booster type, collapse distance, and horn down speed

Booster	1:1 (green) Final amplitude ~ 34 $\mu\text{m}_{p-p}$	1: 0.60 (purple) Final amplitude ~ 20.4 $\mu\text{m}_{p-p}$
Collapse distance (mm)	0.20, 0.30, 0.40	0.20, 0.30, 0.40
Horn down speed (mm/s)	0.05, 0.10, 0.15, 0.20	0.05, 0.10, 0.15, 0.20

**Fig. 4** (a) Representative image of samples with excessive flashes and deformed areas (circled) after USV application; (b) samples without any physical deformation/distortion after USV application, post-tensile testing (200N TF, 0.15 mm/s down speed, 0.30 mm collapse distance, 1:0.60 booster)



of a magnesium alloy was studied [29]. It was observed that a lower amplitude of USV helped softening of material and increased the formability while the higher amplitude decreased the plasticity. In our study, 1:0.60 ratio booster produced less amplitude than 1:1 ratio booster. We infer that using less amplitude might have helped in plasticizing the material in between the printed layers and increased the tensile strength through interdiffusion and re-entanglement of polymer chains.

After analyzing the tensile strengths of 1:0.60 ratio booster, it was identified that a combination of 0.15 mm/s horn down speed and 0.30 mm collapse distance yielded the highest tensile strength. By using this set of parameters, the next set of experiments was performed by changing only the TF. Four different TFs (150, 175, 225, 250 N) were used to apply USV and the tensile strengths were compared with the 200 N samples. Among the TF values, the highest tensile strength was observed for 200 N TF samples. Wang et al. investigated the effect of several ultrasonic welding parameters including TF on short carbon fiber reinforced Nylon 6 composite plates [30]. A TF of 200 N produced the highest temperature and bonding efficiency in their study. In their study, it was hypothesized that too high of a TF might have squeezed some material out and lowered the bond strength. Therefore, the same hypothesis may apply to our study as well. While higher than 200 N TF may have led to material squeeze out, lower TF might not have been strong enough to produce any superior results. The parameters of 200 N TF, 0.15 mm/s horn down speed, and 0.30 mm collapse distance were used for the rest of the experiments in this study because this parameter combination did not cause any major physical deformation/distortion while it also enabled an increase in tensile strength of the specimens.

## 4.2 Effect of ultrasonic on both sides

One of the goals of the study was to differentiate between the effects of one-side ultrasonic application compared to the application on both sides. To document the structural differentiation between one-side and both-side ultrasonic application on specimens, X-ray CT was used. The samples from this section and afterwards were printed using LulzBot 3D printer. Samples for this part of the study were printed using the “lines” pattern, 0.20 mm layer height, and at 100% infill density with rafts. One sample was subjected to USV on one side and another one on both sides. These along with the control sample (no ultrasonic) were observed through X-ray CT. Figure 5 displays the side view of the three samples’ gauge areas. The images were cropped from the same section of the samples at the same magnification. It can be noticed that, for control and one-sided ultrasonic samples, the voids in between layers are more visible than the both-side ultrasonic sample. This suggests that the application of USV on both sides of the sample helped to consolidate the layers more. As the application of ultrasonic on only one side of the samples led to fewer gaps in-between the rasters and more fusion of layers in another study [31], we can infer that applying ultrasonic on both sides can reduce the voids even more and improve layer adhesion further.

## 4.3 Effect of both-side ultrasonic application on samples with different layer heights

Based on the observation from X-ray CT, further investigation was performed to characterize the effect of both-side USV on samples with different layer heights. We hypothesized that for samples of larger layer heights, both-side applications of USV could increase the tensile strength

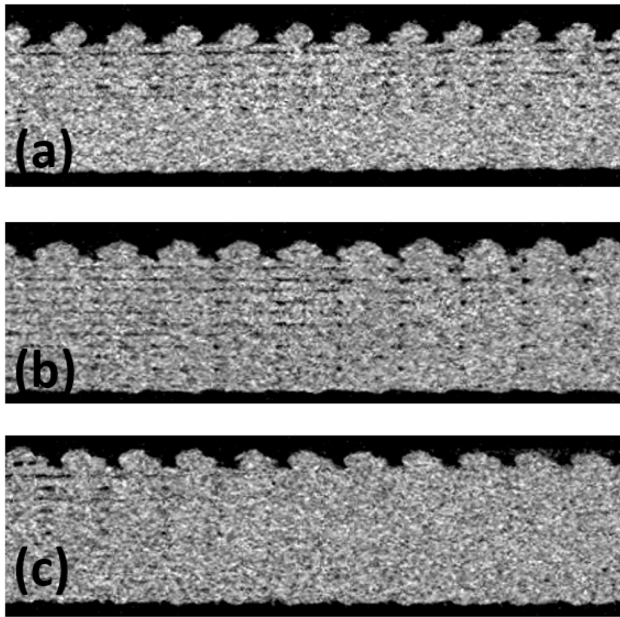
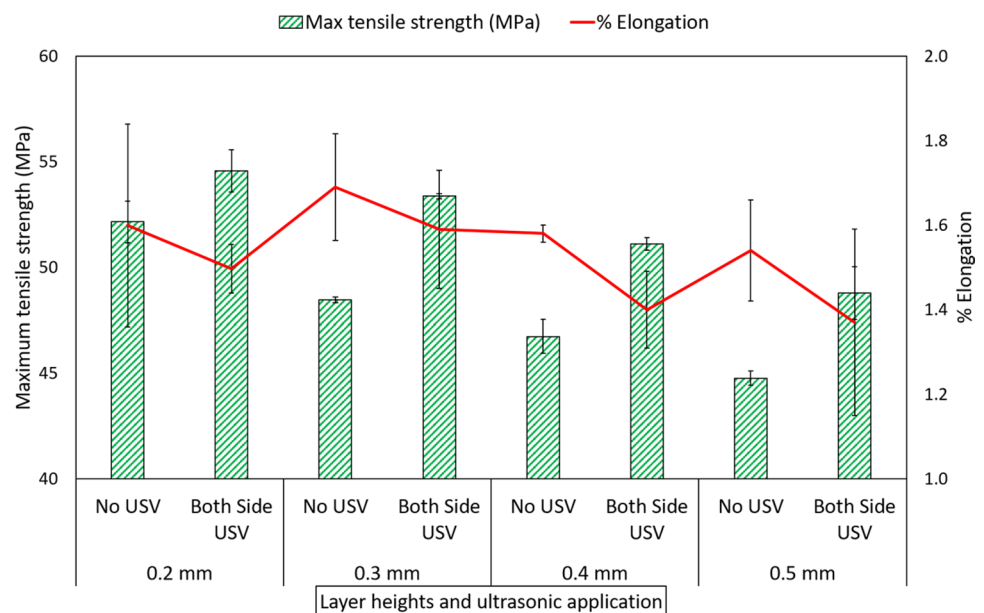


**Fig. 5** Comparison of FDM samples using X-ray CT; (a) control, (b) one-side USV application, and (c) both-side USV application (top sides of each sample represent top surfaces of the samples)

more than that of samples with smaller layer heights. In general, FDM samples with smaller layer heights have higher tensile strength. Figure 6 shows the maximum tensile strength and % elongation of samples without ultrasonic and after applying ultrasonic on both sides. The samples were printed at 4 different layer heights using the “lines” pattern and 100% infill density. It can be noticed that for each layer height, ultrasonic application on both sides of the samples increased the tensile strength. The

**Fig. 6** Tensile property of samples as a function of USV application scenario and layer height (error bars represent standard deviation)



increase of tensile strength ranged from 5 to 10% but the highest % increase was observed for samples printed with 0.30 mm layer height and the lowest for 0.20 mm layer height. As a layer height of 0.20 mm was small enough to produce a dense solid structure, the possibility of increasing the tensile strength even further was low. Layer height of 0.30 mm was more suited for improving tensile strength through ultrasonic application. Samples with layer height more than 0.30 mm produced a very similar % increase in tensile strength as 0.30 mm samples. Maybe a more tailored USV parameter for 0.40 mm and 0.50 mm samples could have led to further increase in tensile strength. As expected, both-side applications of ultrasonic made the samples less ductile which is evident with lower % elongation for both-side samples than the control samples. As for 0.30 mm layer height, the highest % increase in tensile strength was observed, for all the following experiments, 0.30 mm layer height was used.

#### 4.4 Effect of both-side ultrasonic application on different infill patterns and densities

In this section, further investigation was conducted to characterize the effect of internal fill geometry and density on the surface roughness, thickness, and tensile strength of the parts, specifically 3 types of infill patterns (lines, zig-zag, grid) and 3 infill densities (100%, 90%, 80%) were studied. All the samples were printed following this experimental design ( $n = 3$ ). Post-printing, USV was applied on both sides of the samples at 200 N TF, 0.30 mm collapse distance, and 0.15 mm/s horn down speed using the 1:0.60 booster.



#### 4.4.1 Surface roughness

Two-way ANOVA demonstrated that application of both-sided USV significantly affected the surface roughness of the samples. Interactions between USV and other factors were also statistically significant except for the interaction between infill density and USV application. In FDM, the top and bottom layers of a part have 100% infill solid shell structure irrespective of the infill density of the other layers, which was the reason behind this insignificant result. Figure 7 displays the average roughness values for different densities, patterns, and sides. It can be noticed that the surface roughness decreased in all cases but the % decrease was higher for top surfaces than the bottom surfaces. For the “lines” pattern, highest decrease in surface roughness of 59% and 47% was observed on top side of 80% infill and bottom side of 100% infill samples respectively. Maximum reduction in average roughness of 70% and 22% was observed on top and bottom sides of 100% density “zig-zag” infill samples. Roughness values of “grid” pattern samples showed the highest decrease for 80% infill samples and it was 70% and 53% decrease on top side and bottom side respectively. Similar reduction in surface roughness of FDM samples after ultrasonic application was reported by Li et al. [17], while in another study, a piezoelectric ultrasonic transducer was mounted on the printer bed and the effect of different frequency vibrations on the surface finish of FDM samples was studied. It was found that ultrasonically vibrating the printer bed during the FDM process improved the surface finish of the samples [32].

#### 4.4.2 Thickness

Results from two-way ANOVA showed that both-sided USV and its interactions with other factors significantly affected the thickness of the samples. But, the overall decrease in thickness after both-sided USV was less than 5.20% which is within inherent dimensional variations typically observed in parts fabricated with standard FDM-based AM methods. For example, in a study by Alafaghani et al., ASTM D638 Type IV samples were printed by changing several FDM parameters including layer height, infill density, and infill patterns. The dimensions of the printed samples were compared with the designed model and it was observed that the thicknesses of all the samples increased after FDM [33]. Based on this observation, we can deduce that, in our study, both-sided USV is actually compressing the part back to its designed thickness. Figure 8 displays the comparison of thickness before and after ultrasonic application. In general, it was noticed that the thickness of the samples increased with the increase in infill density. Also, the thickness of the samples decreased for all infill densities regardless of the infill pattern after the USV was applied. Samples with “lines”

pattern infill and 90% infill density had the highest 5.20% reduction and 80% infill “zig-zag” samples had the lowest reduction of 2%. This observation of decreased thickness of the samples is in alignment with the trends found in published literature. Li et al. applied USV on FDM-printed ABS (acrylonitrile butadiene styrene) and PLA samples. While a slight reduction in thickness was observed for ABS samples, almost 10% thickness reduction occurred in PLA samples. Wu et al. studied the bending and dynamic mechanical properties of ABS after applying USV on FDM samples. A 3% thickness reduction was observed after ultrasonic application but the lengths and widths were unchanged [34]. The decrease in thickness is an indicator of layer compression because of ultrasonic-generated heat and downforce resulting in squeeze flow of material at the interface of two adjacent layers following the phenomena described in Section 2, specifically using Eqs. 1, 2, and 3.

#### 4.4.3 Tensile properties

Two-way ANOVA showed that both-sided USV application as well as the interaction between infill pattern and USV significantly affected the maximum tensile strengths. However, the interaction between infill density and USV did not affect the maximum tensile strength significantly. From Fig. 9, it can be noticed that for almost all the control samples the standard deviation is very high. But, after USV application, the variation in tensile strength decreased greatly. We hypothesize that both-sided USV compressed the layers hence creating a more dense and compact structure with more consistent tensile strengths but did not increase the strengths enough to be statistically significant compared to the control samples. From Fig. 9, it is evident that the tensile strengths of the samples with “lines” and “grid” patterns were significantly increased after USV was applied on both sides for all infill densities. The highest % increase was observed for grid pattern samples: 14.18% for 80% infill, 10.65% for 90% infill, and 15.31% for 100% infill. For the “zig-zag” pattern, the tensile strengths did not increase for 90% and 100% infill density. As each infill pattern possesses unique characteristics, the constant set of ultrasonic parameters used in this particular study might not have been suitable for “zig-zag” pattern to produce better results. Further investigation of tensile test data revealed that after USV was applied, the tensile strength for 90% and 80% infill density samples was close to the tensile strength of 100% infill samples. It can be inferred from this information that by printing at a lower infill density and applying USV, tensile strength similar to post-ultrasonic 100% density samples can be achieved. Moreover, for samples printed with “lines” and “grid” patterns, post-ultrasonic tensile strengths of 80% and 90% infill sets were higher than 100% infill control samples. These results show that the ultrasonic

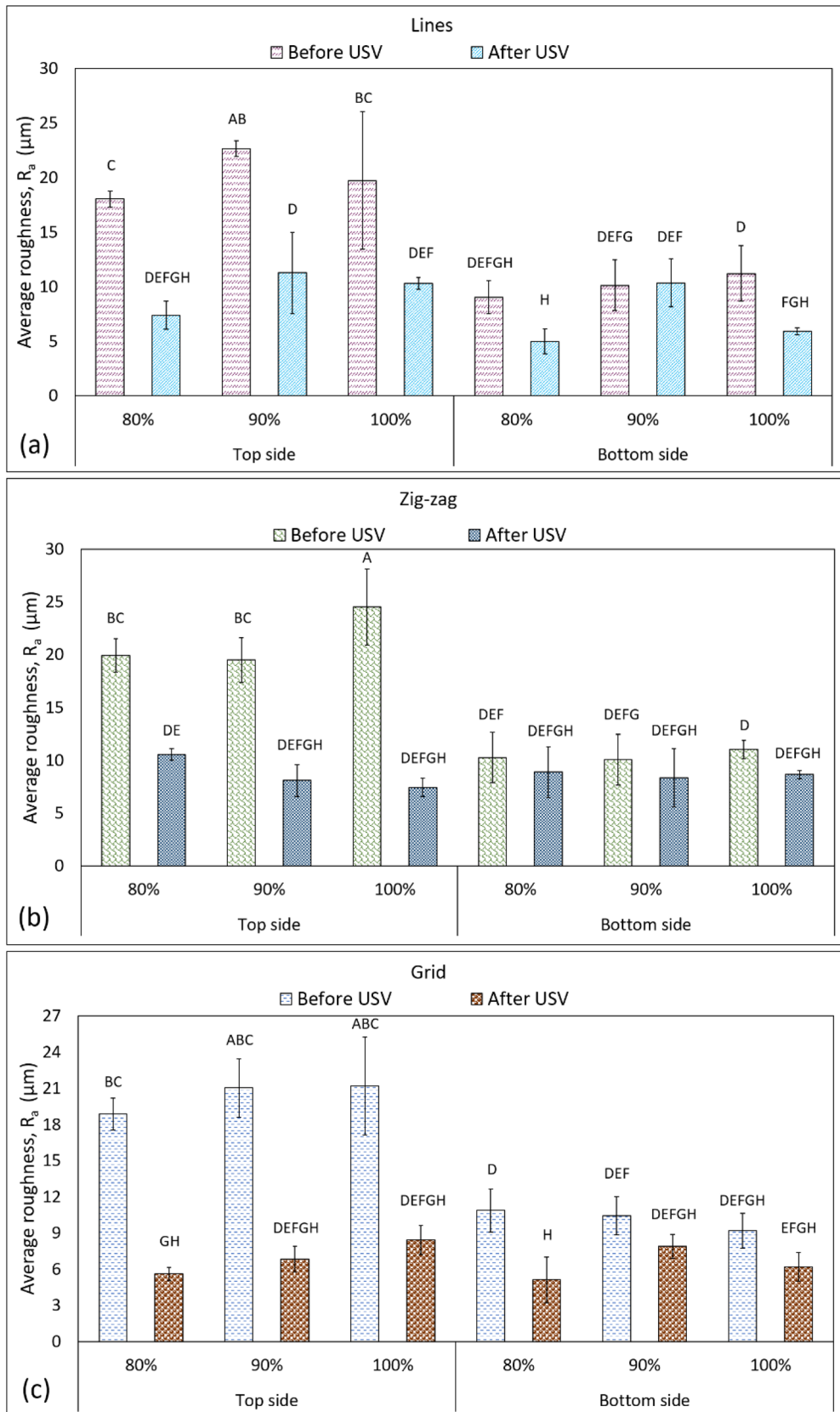


**Fig. 7** Average surface roughness of samples before and after application of both-side USV (printed in 3 patterns and 3 infill densities-error bars represent standard deviation) (levels not connected by same letter are significantly different)

**Fig. 8** Average thickness of samples before and after application of both-side USV (printed in 3 patterns and 3 infill densities-error bars represent standard deviation) (levels not connected by same letter are significantly different)

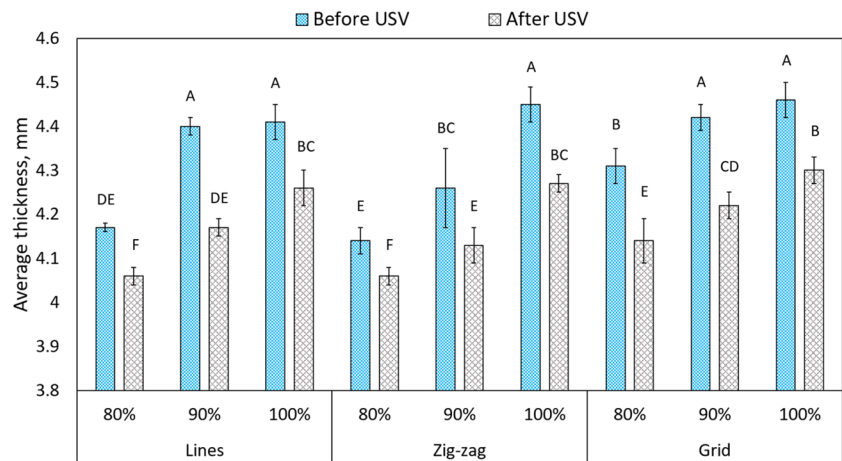
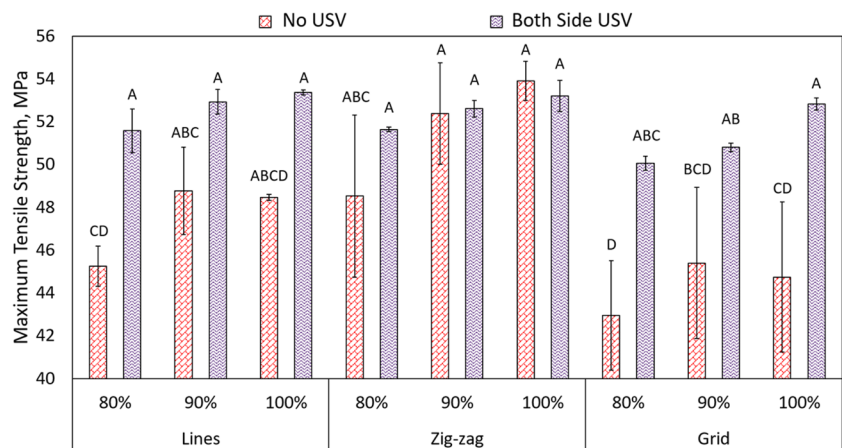


**Fig. 9** Maximum tensile strengths of samples as a function of USV application scenario (printed in 3 patterns and 3 infill densities-error bars represent standard deviation) (levels not connected by same letter are significantly different)



strengthening of FDM samples through which less material can be used during printing resulting in lower print time and material cost but higher tensile strength can be achieved. Similar results have been documented by Li et al. who studied the strengthening effect of USV on FDM-printed ABS samples by using a controlled variate method [17]. Up to 11.3% increase in tensile strength was observed after applying USV using different parameter values. In another study, the effect of USV on the mechanical properties of an amorphous (ABS) and a semi-crystalline polymer (PLA) was explored extensively [31]. The tensile strength of ABS and PLA was increased by 12.94% and 22.83% respectively. Increased interdiffusion and polymer chain entanglement between rasters due to ultrasonic heat generation was credited for the improved tensile strength in both studies. In the study by Wu et al. on USV on FDM, it was observed that for samples printed using 12 μm ultrasonic amplitude, the tensile strength was increased by 13.2% [35]. This observation was attributed to the increased crystallinity of the samples because of higher intramolecular heat generation during ultrasonic application.

A similar approach was taken by Maidin et al. where two piezoelectric transducers were attached in two corners of a printer bed and a function generator was used to supply USV at different frequencies during printing samples using recycled ABS filament [36]. The ultimate tensile strength of samples printed at 20 kHz frequency increased by 18.59% and samples printed at 10 kHz frequency had an increase of 11.03%. Their study demonstrated that by using USV, the mechanical properties of recycled materials could be improved which helps in sustainable reuse of waste plastics. The interlayer adhesion strength of FDM-printed two-layer trouser peel test samples was investigated by Tofangchi et al. [37]. They compared the samples printed with traditional printhead with the samples printed with ultrasound transducer attached printhead. Up to 10% increase in interlayer adhesion was observed for ABS samples that were printed using 34.4 kHz ultrasonic vibration. Increased reptation and polymer chain entanglement due to ultrasonic application-induced increase in chain relaxation was attributed for the improved interlayer strength.

#### 4.4.4 SEM image analysis

SEM was used to observe the fracture surface of the samples without and with ultrasonic applied on both sides. Figure 10 displays the samples printed with a “grid” pattern at 90% infill density. We could identify several layers in the cross-section of the sample without ultrasonic application as shown in Fig. 10(a) but the number of layers that can be distinguished in the cross-section after ultrasonic application was lower as presented in Fig. 10(b). This observation can be attributed to the layer consolidation due to USV.

A similar outcome was observed for samples printed with a “zig-zag” pattern at 80% infill density (Fig. 10(c), (d)). The layers were completely unidentifiable after USV was applied. Figure 10(e) and (f) display the “zig-zag” 100% samples fracture surfaces without and with ultrasonic. In the sample that received USV (Fig. 10(f)), the fracture surface became very smooth indicating an

extremely brittle fracture. Figure 10(d) looks very similar to Fig. 10(e) which indicates that after ultrasonic application, the 80% infill density samples acted almost similar to the 100% infill density control FDM sample. The observed consolidation of layers is the result of welding occurring between the layers inside the samples. Equation 11 is the governing equation for determining the final degree of welding and it is evident that temperature at a specific time interval plays a crucial role. The images in Fig. 10 are proof of interlayer welding where the combination of time and temperature worked best for the respective set of samples. We also observed that in a specific time duration, increasing the material temperature by changing amplitude increases the degree of welding which will be presented in a future publication. Similar layer consolidation or increased fusion between rasters due to applied USV was observed by examining the fracture surfaces using the SEM technique in multiple studies [17, 31, 34, 35].

**Fig. 10** SEM images of fracture cross-sections without and with USV application: (a) and (b) grid 90%, (c) and (d) zig-zag 80%, and (e) and (f) zig-zag 100% samples (left side images represent samples without USV)

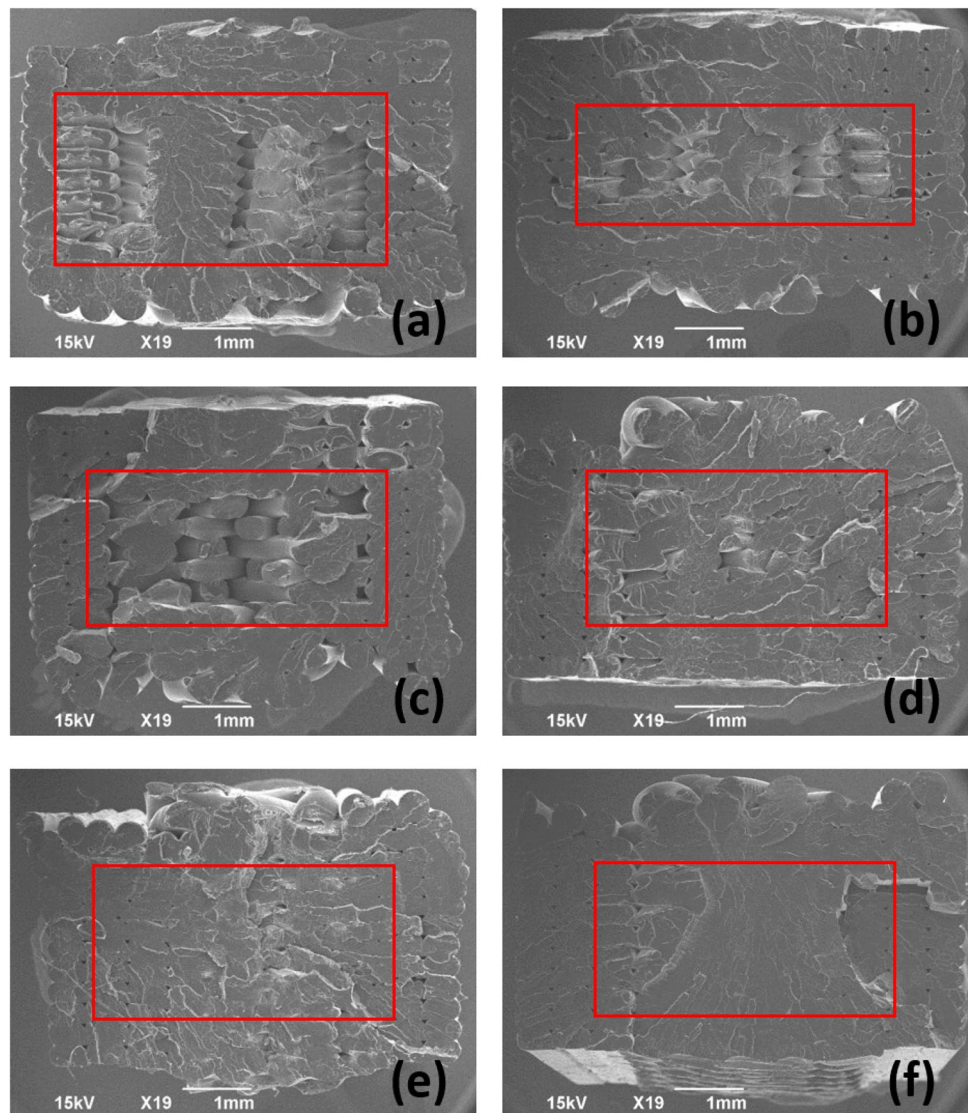
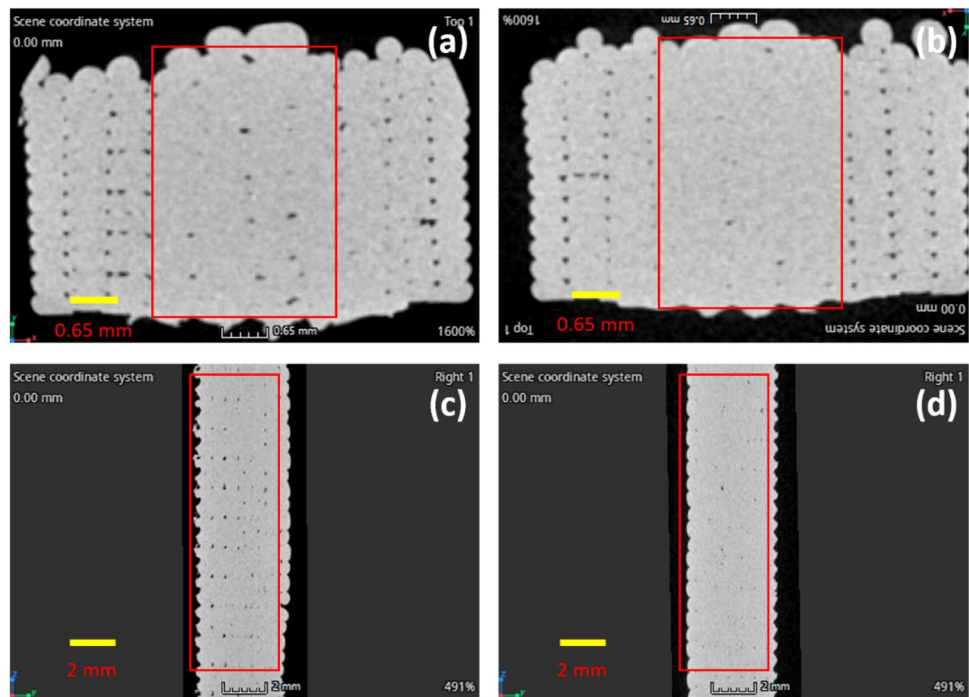


**Fig. 11** X-ray CT observation of samples without USV and with USV application: top row represents cross-section images (a) control (b) post-USV; bottom row represents side view (c) control (d) post-USV (images are from “Grid-100%” samples)



#### 4.4.5 X-ray CT observation

To observe the effect of ultrasonic on the voids in FDM samples, X-ray CT was used. X-ray CT can reveal the internal details of objects in three dimensions non-destructively. The mid-point cross-section of samples both length-wise and width-wise was captured for the illustration purpose from the digital images using myVGL. Figure 11 shows the cross-section of the “grid” 100% infill samples. It can be noticed that, compared to the control sample, the total volume of the voids was less in the sample that had ultrasonic applied on both sides. This observation corroborates the fact that USV can be used to minimize the process inherent voids found in FDM samples. Li et al. also illustrated the void reduction phenomenon in their work and attributed this to the increased interdiffusion and polymer chain re-entanglement after applying USV [31].

## 5 Conclusion

In this study, we characterized the effect of USV on the physical, tensile, and morphological properties of ASTM D638 Type IV samples printed using the FDM method. A collapse distance of 0.30 mm, down speed of 0.15 mm/s, TF of 200 N, and 1:0.60 (purple) booster were identified to be the optimum parameter combination through screening experiments. Comparison of one-sided versus both-sided USV application using X-ray CT showed that both-sided USV reduced interlayer voids more effectively.

Subsequently, the effect of both-sided USV on the tensile strength of FDM samples printed with different layer heights was characterized. After that, the impact of applying both-sided USV on FDM samples with different infill patterns and densities was investigated. Three types of infill patterns (grid, line, zig-zag) and densities (80%, 90%, 100%) were analyzed for surface roughness, thickness, and tensile properties compared to control samples. Decrease in post-ultrasonic surface roughness was observed (maximum 70% decrease) where % decrease was much higher on top sides than the bottom sides owing to having the raft on the bottom side. Tensile strengths increased after USV application for line and grid pattern samples regardless of density (highest 15.31% increase). Notably, post-USV tensile strengths of lower density samples became comparable to higher density samples. SEM and X-ray CT images showed enhanced layer consolidation and void reduction due to USV-induced squeeze flow and interfacial healing.

This research presents the potential of USV as a post-processing technique for enhancing FDM parts made from PLA, a widely used bio-based plastic. Despite PLA’s inherent low strength, this study suggests that USV treatment could extend its utility to applications requiring medium to high strength. The proposed methodology could also benefit other bio-based materials suitable for high-strength applications. Moreover, this study demonstrates the possibility of integrating USV as a secondary processing step during FDM. While the current approach involved post-processing by applying USV to finished samples, there were issues regarding uniform distribution of force and vibration. To

address these issues, our ongoing work aims to implement USV application every few layers in a scanning mode during printing. The findings of this in-progress project will be published in the near future.

**Acknowledgements** We would like to thank Mr. Leo Klinstein from Dukane Corporation and Mr. Bill Reed from Branson/Emerson Ultrasonics for providing guidance and resources to conduct this study.

**Author contribution** Raihan Quader: methodology, investigation, visualization, and writing—original draft preparation. Leo Klinstein: methodology. David Grewell: conceptualization and funding acquisition. Lokesh Karthik Narayanan: conceptualization, funding acquisition, methodology, investigation, validation, and writing—review and editing.

**Funding** This study was supported by a grant from the National Science Foundation-Industry University Cooperative Research Center (NSF/IUCRC)- Center for Bioplastics and Biocomposites (CB2) (Award #2021C3).

## Declarations

**Conflict of interest** The authors declare no competing interests.

**Open Access** This article is licensed under a Creative Commons Attribution 4.0 International License, which permits use, sharing, adaptation, distribution and reproduction in any medium or format, as long as you give appropriate credit to the original author(s) and the source, provide a link to the Creative Commons licence, and indicate if changes were made. The images or other third party material in this article are included in the article's Creative Commons licence, unless indicated otherwise in a credit line to the material. If material is not included in the article's Creative Commons licence and your intended use is not permitted by statutory regulation or exceeds the permitted use, you will need to obtain permission directly from the copyright holder. To view a copy of this licence, visit <http://creativecommons.org/licenses/by/4.0/>.

## References

- Wang X, Jiang M, Zhou Z et al (2017) 3D printing of polymer matrix composites: a review and prospective. *Compos B Eng* 110:442–458. <https://doi.org/10.1016/j.compositesb.2016.11.034>
- Wong KV, Hernandez A (2012) A review of additive manufacturing. *ISRN Mechanical Engineering* 2012:1–10. <https://doi.org/10.5402/2012/208760>
- Rahim TNAT, Abdullah AM, Md Akil H (2019) Recent developments in fused deposition modeling-based 3D printing of polymers and their composites. *Polym Rev* 59:589–624
- Lyu Y, Chen Y, Lin L, et al. (2022) Architecture of covalent bonds between filament layers to enhance performance of 3D printing biodegradable polymer blends. *Polym Test* 106. <https://doi.org/10.1016/j.polymertesting.2021.107456>
- Kim H, Lin Y, Tseng T (2018) A review on quality control in additive manufacturing. *Rapid Prototyp J* 24:645–669. <https://doi.org/10.1108/RPJ-03-2017-0048>
- Sun X, Mazur M, Cheng CT (2023) A review of void reduction strategies in material extrusion-based additive manufacturing. *Addit Manuf* 67:103463. <https://doi.org/10.1016/j.addma.2023.103463>
- Rigotti D (2019) Polymer composites for sustainable 3D printing materials. University of Trento. <http://eprints-phd.biblio.unitn.it/3813/>
- Ahn D, Kweon JH, Kwon S et al (2009) Representation of surface roughness in fused deposition modeling. *J Mater Process Technol* 209:5593–5600. <https://doi.org/10.1016/j.jmatprotec.2009.05.016>
- Sun Q, Rizvi GM, Bellehumeur CT, Gu P (2008) Effect of processing conditions on the bonding quality of FDM polymer filaments. *Rapid Prototyp J* 14:72–80. <https://doi.org/10.1108/13552540810862028>
- Khurana JB, Simpson TW, Frecker M (2020) Structurally intelligent 3D layer generation for active-Z printing. *Solid Freeform Fabrication 2018: Proceedings of the 29th Annual International Solid Freeform Fabrication Symposium - An Additive Manufacturing Conference*, SFF 2018 2413–2426. <https://doi.org/10.26153/tsw/17234>
- Narahara H, Shirahama Y, Koresawa H (2016) Improvement and evaluation of the interlaminar bonding strength of FDM parts by atmospheric-pressure plasma. *Procedia CIRP* 42:754–759. <https://doi.org/10.1016/j.procir.2016.02.314>
- Kishore V, Ajinjeru C, Nycz A et al (2017) Infrared preheating to improve interlayer strength of big area additive manufacturing (BAAM) components. *Addit Manuf* 14:7–12. <https://doi.org/10.1016/j.addma.2016.11.008>
- Ravi AK, Deshpande A, Hsu KH (2016) An in-process laser localized pre-deposition heating approach to inter-layer bond strengthening in extrusion based polymer additive manufacturing. *J Manuf Process* 24:179–185. <https://doi.org/10.1016/j.jmapro.2016.08.007>
- Grewell DA, Benatar A, Park JB (2003) *Plastics and composites welding handbook*. Hanser Publications, München
- Grewell D, Benatar A (2007) *Welding of plastics: fundamentals and new developments*. *Int Polym Proc* 22:43–60
- Lay M, Thajudin NLN, Hamid ZAA, et al (2019) Comparison of physical and mechanical properties of PLA, ABS and nylon 6 fabricated using fused deposition modeling and injection molding. *Compos B Eng* 176. <https://doi.org/10.1016/j.compositesb.2019.107341>
- Li G, Zhao J, Jiang J et al (2018) Ultrasonic strengthening improves tensile mechanical performance of fused deposition modeling 3D printing. *Int J Adv Manuf Technol* 96:2747–2755. <https://doi.org/10.1007/s00170-018-1789-0>
- Quader R, Grewell D, Narayanan LK (2023) Effect of ultrasonic vibration on physical and tensile properties of fused deposition modeled polylactic acid specimens. In: *ASME 2023 18th International Manufacturing Science and Engineering Conference*. <https://doi.org/10.1115/MSEC2023-104816>
- Benatar A, Gutowski TG (1989) Ultrasonic welding of PEEK graphite APC-2 composites. *Polym Eng Sci* 29:1705–1721. <https://doi.org/10.1002/pen.760292313>
- Tolunay MN, Dawson PR, Wang KK (1983) Heating and bonding mechanisms in ultrasonic welding of thermoplastics. *Polym Eng Sci* 23:726–733. <https://doi.org/10.1002/pen.760231307>
- Grewell D, Benatar A (2008) Semi-empirical, squeeze flow and intermolecular diffusion model. I. determination of model parameters. *Polym Eng Sci* 48:860–867. <https://doi.org/10.1002/pen.21021>
- Bird RB, Armstrong RC, Hassager O (1987) *Dynamics of polymeric liquids*. Vol. 1, 2nd Ed. : Fluid mechanics. John Wiley and Sons Inc., New York, NY, United States
- DeGennes PG (1971) Reptation of a polymer chain in the presence of fixed obstacles. *J Chem Phys* 55:572–579. <https://doi.org/10.1063/1.1675789>
- de Gennes P (1983) Entangled polymers. *Phys Today* 36:33–39. <https://doi.org/10.1063/1.2915700>

25. Jud K, Kausch HH, Williams JG (1981) Fracture mechanics studies of crack healing and welding of polymers. *J Mater Sci* 16:204–210
26. Kincs J, Martin SW (1996) Non-Arrhenius conductivity in glass: mobility and conductivity saturation effects. *Phys Rev Lett* 76:70
27. Martin SW, Schrooten J, Meyer B (2002) Non-Arrhenius ionic conductivity in optimized fast ion conducting glasses: application of the Drude model to ion–ion scattering. *J Non Cryst Solids* 307:981–991
28. Bastien LJ, Gillespie JW Jr (1991) A non-isothermal healing model for strength and toughness of fusion bonded joints of amorphous thermoplastics. *Polym Eng Sci* 31:1720–1730
29. Wen T, Wei L, Chen X, Pei CL (2011) Effects of ultrasonic vibration on plastic deformation of AZ31 during the tensile process. *Int J Miner Metall Mater* 18:70–76. <https://doi.org/10.1007/s12613-011-0402-4>
30. Wang Y, Rao Z, Bao S et al (2022) Process and strength analysis of joining CF/PA6 composite plates without energy director by a servo-driven ultrasonic welder. *J Market Res* 19:4613–4626. <https://doi.org/10.1016/j.jmrt.2022.07.010>
31. Li G, Zhao J, Wu W, et al (2018) Effect of ultrasonic vibration on mechanical properties of 3D printing non-crystalline and semi-crystalline polymers. *Materials* 11. <https://doi.org/10.3390/ma11050826>
32. Maidin S, Muhamad MK, Pei E (2015) Feasibility study of ultrasonic frequency application on fdm to improve parts surface finish. *J Teknol* 77:27–35. <https://doi.org/10.11113/jt.v77.6983>
33. Alafaghani A, Qattawi A, Alrawi B, Guzman A (2017) Experimental optimization of fused deposition modelling processing parameters: a design-for-manufacturing approach. In: *Procedia Manufacturing*. Elsevier B.V., 10:791–803. <https://doi.org/10.1016/j.promfg.2017.07.079>
34. Wu W, Jiang J, Jiang H et al (2018) Improving bending and dynamic mechanics performance of 3D printing through ultrasonic strengthening. *Mater Lett* 220:317–320. <https://doi.org/10.1016/j.matlet.2018.03.048>
35. Wu W, Li J, Jiang J, et al (2022) Influence mechanism of ultrasonic vibration substrate on strengthening the mechanical properties of fused deposition modeling. *Polymers (Basel)* 14. <https://doi.org/10.3390/polym14050904>
36. Maidin S, Ting KH, Sim YY (2022) Investigation of mechanical properties of recycled ABS printed with open source FDM printer integrated with ultrasound vibration. *Int J Integr Eng* 14:57–63. <https://doi.org/10.30880/ijie.2022.14.04.006>
37. Tofangchi A, Han P, Izquierdo J, et al (2019) Effect of ultrasonic vibration on interlayer adhesion in Fused Filament Fabrication 3D printed ABS. *Polymers (Basel)* 11. <https://doi.org/10.3390/polym11020315>

**Publisher's Note** Springer Nature remains neutral with regard to jurisdictional claims in published maps and institutional affiliations.